The critical tube diameter and critical energy for direct initiation of detonation in $C_2H_2/N_2O/Ar$ mixtures

Bo Zhang[1†], Hoi Dick Ng[2], John H.S. Lee[3]

[1]Beijing Institute of Technology
State Key Laboratory of Explosion Science and Technology, Beijing, 100081, China

[2]Concordia University
Department of Mechanical and Industrial Engineering
Montréal, QC, H3G 1M8, Canada

[3]McGill University
Department of Mechanical Engineering, Montréal, QC, H3A 2K6, Canada

[†]Corresponding Author

Beijing Institute of Technology
State Key Laboratory of Explosion Science and Technology
Beijing, 100081, China
e-mail: simon_19830915@hotmail.com

Revised manuscript submitted to *Combustion and Flame*
Ms. Ref. No.: CNF-D-11-00342

January, 2012

Abstract

In this study, the dynamic detonation parameters, namely, the critical tube diameter and critical energy for direct initiation, of $C_2H_2/N_2O/Ar$ mixtures were measured at various initial conditions. Using chemical kinetics with the Konnov mechanism and experimental measured data, a simple correlation to evaluate the critical tube diameter of $C_2H_2/N_2O/Ar$ detonation is developed, given by $d_c = 594.8\varphi^{0.623}(1 - X_{Ar})^{0.2176}(p/p^o)^{-0.0246}\Delta_I$ which is applicable for stoichiometric mixtures with initial pressures ranging from 50 to 130 kPa, equivalence ratios from 0.625 - 2.5 and stoichiometric mixtures with maximum percentage of argon dilution up to 50% at the atmospheric pressure. By combining this correlation function with a theoretical model based on a simple work done concept, the critical energy for direct blast initiation can be predicted; and the theoretical predictions are found to be in good agreement with the critical energy measured experimentally. To assess the detonation sensitivity, the critical energy results for direct initiation of detonation in $C_2H_2/N_2O/Ar$ mixtures are compared with those in $H_2/N_2O/Ar$ mixtures [Zhang et al. Int. J. Hydrogen Energy, 39: 5707-5716 (2011)]. The results indicate that $C_2H_2/N_2O/Ar$ is more sensitive than $H_2/N_2O/Ar$ at the same initial conditions. This is also supported qualitatively by the chemical kinetic calculation which shows that the ZND induction length scale for $C_2H_2/N_2O/Ar$ is relatively smaller than that of $H_2/N_2O/Ar$ mixture. Lastly, the effect of the oxidizer on the detonation sensitivity is studied by comparing the critical energy between $C_2H_2/N_2O/Ar$ and $C_2H_2/O_2/Ar$ mixture. It is found that a higher energy is required to successfully initiate a spherical detonation in $C_2H_2/N_2O/Ar$ than in $C_2H_2/O_2/Ar$ mixtures and equivalently, the results agree qualitatively with the ZND induction length analysis.

Keywords: detonation; nitrous oxide; critical energy; critical tube diameter; induction length

1. Introduction

Nitrous oxide (N_2O) is a stable compound that is comparatively unreactive to many substances at room temperature. Its use has been considered in medical application for its anesthetic effects and rocket propulsion research as a cold gas propellant or oxidant [1, 2]. When heated sufficiently, however, N_2O is an energetic oxidizer; It first decomposes endothermically to N_2 and O by the initial decomposition step: N_2O (+ M) $\leftrightarrow$ N_2+ O (+ M) and subsequently energy release can be driven by oxygen atoms combination: O + O (+ M) $\leftrightarrow$ O_2 (+ M). Thus, N_2O mixed with other gaseous fuels can potentially lead to various accidental explosions [3, 4]. Therefore, it is necessary to understand the subject of nitrous oxide explosion properties and to assess its potential hazards.

For the past decades, many studies have been devoted to explore the combustion properties such as ignition delay times, flame burning speeds, flammability limits and detonation cell sizes in hydrogen-nitrous oxide-diluent mixtures [5-13]. These studies were mostly motivated by the concern of hazards posed by the accidental explosions in these H_2/N_2O gaseous mixtures that are continuously generated from stored wastes of military nuclear processes [14-16]. Unlike common hydrocarbon fuel-oxygen or hydrocarbon fuel-air mixtures, the detonation phenomenon in hydrocarbon fuel-nitrous oxide mixtures, e.g., C_2H_2/N_2O considered in this study, has not been widely investigated. Such studies could have an impact of improving the safety in industrial sectors that deals with nitrous oxide from waste treatments, emissions from energy sources or chemical processes [17], and the application of nitrous oxide as an oxidizer, for example in chemical rocket engines [2]. Among different detonation parameters, evaluation of critical diameter and critical energy for direct initiation provides direct means to assess the detonation sensitivity of a given mixture [18, 19] and yet, data on these dynamics parameters for hydrocarbon fuel-nitrous oxide mixtures are rather scarce. Although detonation cell size is also often considered as an important dynamic parameter to quantify the detonation sensitive of a given explosive, it was found that fuel-N_2O mixtures tend to be very unstable with highly irregular cellular structures. For example in $C_2H_2/N_2O/Ar$ mixtures, even with the argon dilution up to 50%, Libouton et al. [20, 21] observed “substructure" with cell sizes of multiple scales, which makes the determination of the cell size for $C_2H_2/N_2O/Ar$ mixtures very difficult.

In this study, we focus on the $C_2H_2/N_2O/Ar$ systems as an example in investigating the effect of nitrous oxide on the sensitivity of detonation formation in hydrocarbon fuel mixtures. Critical tube diameter and critical energy for direct initiation data for $C_2H_2/N_2O/Ar$ mixtures are experimentally obtained at different initial conditions to look at the effects of the initial pressure, equivalence ratio and the amount of argon dilution on the detonation dynamic parameters. These results are then compared with those for $H_2/N_2O/Ar$ to study the influence of hydrogen as a fuel, and compared with $C_2H_2/O_2/Ar$ mixtures to observe the detonation sensitivity if nitrous oxide is being used as an oxidizer. To investigate the detonation sensitivity from chemical kinetics consideration, an induction zone length analysis is also carried out in parallel to support the experimental observations.

2. Experimental details and chemical kinetic analysis

2.1 Experiment setup

Measurement of the critical tube diameter and critical energy were both carried out in a modified spherical bomb apparatus as shown in Figs. 1 and 3, respectively. The original spherical chamber is 8” in diameter and 2” in wall thickness. In both experiments, each explosive mixture was first prepared beforehand in a separate vessel by the method of partial pressures. The storage pressure was kept at 2 atm and the gases were allowed to mix in the vessel for at least 24 hours in order to ensure homogeneity for each experiment.

For the critical tube diameter measurement of $C_2H_2/N_2O/Ar$ mixtures, experiments were carried out in a setup consisted of a vertical circular steel tube connected to a spherical bomb chamber (see Fig. 1). The tube diameters were varied via inserting smaller diameter tubes. The tube diameters used in the experiment were d = 19.1 mm, 15.5 mm, 12.7 mm and 9.13 mm. The initial conditions of the critical tube diameter experiment are shown in Table.1. For each test, the detonation was initiated by a high voltage spark ignition source at the top of the vertical circular steel tube and the wave subsequently transmitted into the spherical chamber. A photo probe and a shock pin were mounted at the top and bottom of the spherical bomb, which were used to determine the time-of-arrival (TOA) signal of the wave. The successful or unsuccessful detonation when it transmits into spherical chamber can be estimated by the TOA signal (see [22] for further details). For completeness, typical traces for a successful detonation transmission from the small circular steel tube (d = 19.1 mm) to the spherical chamber with relatively much larger space, i.e., for $d > d_c$, in a stoichiometric C_2H_2/N_2O mixture at an initial pressure of p_0 = 58 kPa is shown in Fig. 2. It can be seen from Fig. 2 that at this initial pressure, the arrival time of the wave at the photo probe is 206.8 μs and 332.1 μs at the shock pin. The velocity of the wave is calculated to be 2021.3 m/s and 2002.4 m/s in the vertical tube and spherical chamber, which is approximately 90.8% and 90% of the CJ detonation velocity, respectively. It shows that at an initial pressure of 58 kPa, the tube diameter is above the critical value, thus the planar detonation can successfully transmit into a spherical detonation. On the other hand, for an unsuccessful transmission with an initial pressure lower than the critical value, e.g., p_0 = 52 kPa, although a detonation wave still formed in the vertical tube, the detonation failed after exiting into the free space. At this initial pressure, the wave first reached the photo probe at t = 211.2 μs, and the shock pin at t = 1180 μs. With these TOAs from the traces, the velocity of wave in the vertical tube is roughly about 90% CJ and in the spherical bomb the velocity is estimated to be around 11.4% CJ, which clearly indicates failure of the wave. For each successful and unsuccessful initiation of spherical detonation at least 3 shots were repeated to confirm the critical pressure that can form a spherical detonation at each tube diameter.

As for the critical energy measurement, direct initiation of spherical detonations was achieved via a spark discharge from a high voltage and low inductance capacitor inside the closed spherical bomb chamber shown in Fig.3. In brief, the ignition system consists of a high voltage power supply, capacitor bank, a gap-switch, a trigger module (TM-11A) and a slender coaxial electrode mounted on top of the explosion sphere. At the end of this slender electrode there is a 3.5 mm spark gap through which the energy is delivered inside the chamber through the ignition circuit. A PCB piezoelectric pressure transducer is mounted in the wall of the chamber to measure the time of arrival of the wave front. From the arrival time of pressure signal it can be determined whether there is a successful direct initiation of detonation or not. The procedure to distinguish detonation initiation as well as details to estimate the actual spark discharge energy from the ignition system can be found in authors' previous studies [23-28]. In this study, a wide range of initial conditions of $C_2H_2/N_2O/Ar$, $H_2/N_2O/Ar$ and $C_2H_2/O_2/Ar$ mixtures were used, which are summarized in Table 2.

2.2 Chemical kinetics modeling

To investigate the detonation sensitivity of mixtures under different conditions, some aspects of chemical kinetics (i.e., induction length analysis) was also considered [29]. The induction length analysis also provides some insights to explain qualitatively the variation of critical initiation energy and critical tube diameter observed in the experiments. The one-dimension ideal ZND model is used to calculate the characteristic induction length scale and the solutions were computed using the CHEMKIN package [30]. For $C_2H_2/N_2O/Ar$ and $C_2H_2/O_2/Ar$ mixtures, the Konnov chemical kinetic mechanism [31] was used. The version of Konnov mechanism used in this work contains 1016 reactions and 122 species (Release 0.3). This version of the Konnov mechanism has been validated with experimental data for oxidation, ignition, and flame structure of small hydrocarbon and also cases with nitrous oxide [31]. It was largely revised using the data from [32] for acetylene oxidation. In addition, other version of Konnov mechanism is often chosen for detonation analysis in the literature [27, 33-35]. Release 0.4 of the Konnov mechanism was also validated through the comparison of constant volume explosion simulation and available shock tube ignition data for ethylene, propane and hydrogen [36]. For mixtures with N_2O, the sub-mechanism of nitrogen chemistry in the Konnov mechanism is developed on the basis of the widely used Miller-Bowman mechanism [37] with additional reactions and updates. It is worth noting that the Miller-Bowman mechanism is also considered in [6, 13] as the basis and modified for studying detonations in mixtures containing nitrous oxide. For $H_2/N_2O/Ar$ mixtures, the reaction mechanism constructed by Mével et al. [8] was used, which had been well validated with several fundamental combustion problems including ignition delay time and laminar flame speed [8-9], and prediction of detonation properties such as detonation cell size and critical initiation energies [10, 25]. It is worth noting that this chemical kinetic model, constituted of 203 reactions and 32 species, has also been constructed from the mechanisms of Konnov [31] and of Mueller et al. [38]. Comparison for H_2/N_2O mixtures was made in this study between the Mével et al. mechanism and the Konnov mechanism; results can be found in the supplemental materials of this paper. It is found that the difference is not substantial and qualitatively the variation remains essentially the same. Results for C_2H_2/O_2 mixtures were also compared between several other mechanisms with nitrogen chemistry with the Konnov model and the difference seems reasonable, although the Konnov mechanism appears to estimate a smaller ZND induction zone length. Furthermore, results obtained for C_2H_2/O_2 mixtures using different versions of Konnov mechanism (Release 0.3, 0.4 and 0.5) are very close to each other. However, for C_2H_2/N_2O mixtures there seems to have no convergence in the results. Unfortunately, to the author's knowledge, there is no experimental data such as shock tube ignition measurement available for $C_2H_2/N_2O/Ar$ mixtures for direct comparison. It is thus difficult to identify which chemical kinetic mechanism is particularly suitable for $C_2H_2/N_2O/Ar$ mixtures and used for this study. Therefore, due to its reasonable prediction for $H_2/N_2O/Ar$ and $C_2H_2/O_2/Ar$ mixtures and for consistency purpose, the Konnov mechanism (Release 0.3) was kept for all the calculations in this work for the acetylene-based mixtures and Mével et al. mechanism for $H_2/N_2O/Ar$ mixtures.

3. Results and discussion

3.1 $C_2H_2/N_2O/Ar$ critical tube diameter measurement and prediction

Experimental data on the critical tube diameter for C_2H_2/N_2O mixtures at different initial conditions are presented in Figs. 4 and 5. Fig. 4 first shows the variation of tube diameter versus the critical pressure – above which the planar detonation can successfully transmit into an unconfined spherical detonation – for non-diluted C_2H_2/N_2O mixtures at different composition. The critical condition was determined by carrying out the experiment several times at the same condition (e.g., same p_o). It occurred that at initial pressures near the critical value for a given tube diameter, mixed results were obtained (i.e., sometimes GO, sometimes NOGO at the same initial pressure p_o). Therefore, the error bars shown in the plots covered the range of the mixed results. The upper and lower error bars show the initial pressures above or below which no failure or successful transmission were observed, respectively within the number of shots performed at each condition. From Fig. 4, it is of interest to note that C_2H_2/N_2O at $\varphi = 2.5$ is the most sensitive mixture among all the compositions considered here. Similarly, Fig. 5 shows the experimentally measured critical tube diameter as a function of the amount of argon dilution. For 50% argon diluted mixtures, part of the experimental results were extracted from Laberge at al. [39], which follows well the trend of the present data with tube diameter smaller than 20 mm. In general, the results show that with increasing amount of argon dilution, the critical tube diameter increases consequently at the same initial pressure.

In these plots, correlations are also included for qualitative comparison and to further elucidate the trend of variation. The correlation is based on the consideration that the detonation front can be characterized by a characteristic reaction zone length, and the diffraction process is governed physically by the tube diameter. Dimensional consideration thus suggests a correlation between these two characteristic length scales. Using the Konnov chemical reaction mechanism for $C_2H_2/N_2O/Ar$ mixtures, the induction zone length of a steady ZND detonation structure can be computed, which can be used to scale the critical tube diameter with $d_c = A \cdot \Delta_I$. Using the experimentally measured critical tube data, an empirical expression for computing the proportionality parameter A has been determined – a mathematical form similar to those used in [10, 25] for detonation cell size correlation. A is expressed as a function of equivalence ratio φ, argon diluent mole fraction X_{Ar}, and ratio of initial pressure to standard pressure p/p^o:

$$A = 594.8\varphi^{0.623}\left(1 - X_{Ar}\right)^{0.2176}\left(p / p^{o}\right)^{-0.0246} \quad (1)$$

For the above correlation, the coefficient of determination R^2, and the maximum deviation between the correlated values and the experimental data are 0.909 and 10.67%, respectively. Thus, it can be seen that the correlation from the $d_c = A \cdot \Delta_I$ relationship is in fairly good agreement with the experimental data. This expression provides a reasonable estimation of critical tube diameter for $C_2H_2/N_2O/Ar$ mixtures within the range of initial pressures from 50 to 130 kPa at stoichiometric condition, equivalence ratio from 0.625 - 2.5 and with maximum percentage of argon dilution in stoichiometric $C_2H_2/N_2O/Ar$ mixtures up to 50% at atmospheric pressure. By using the correlation the critical tube diameter of C_2H_2/N_2O could also be approximated for conditions beyond the range of experimental measurement. This correlation will be used as input to a model in the following section to predict theoretically another dynamic parameter – the critical initiation energy.

3.2 $C_2H_2/N_2O/Ar$ critical initiation energy measurement and prediction

Fig. 6 shows the critical energy as a function of initial conditions obtained from both experimental measurement and theoretical prediction for the stoichiometric C_2H_2/N_2O mixture. Similarly, the upper and lower limits of the error bar represent respectively the last energy values used in an experiment with the same conditions at which successful and failure of direct initiation are observed. This representation was also accepted in our previous papers on the problem of direct initiation of detonation [25, 27]. In general, similar to common fuel-oxygen mixtures, by increasing the initial pressure the critical energy decreases. For the theoretical prediction, result is obtained using a work done model and the $d_c = A \cdot \Delta_I$ critical tube correlation obtained in Section 3.1. The work done concept [18, 28, 40-41] is essentially based on a piston model. Assuming the planar detonation wave as an interface or a piston propagating at constant velocity and transmitting into an unconfined space, its work done can be given by:

$$E_c = \int_0^{t^*} p_{CJ} S(t) u_{CJ} dt \tag{2}$$

where p_{CJ} , u_{CJ} denote the CJ detonation pressure and particle velocity, respectively. t^* is the time when the rarefaction wave reaches the tube axis, $t^* = d_c/2a_{CJ}$ with a_{CJ} being the sound speed of the detonation products [18, 42]. $S(t)$ is the surface area of the planar CJ detonation wave in the confined tube, which is written as:

$$S(t) = \pi \left(\frac{d_c}{2} \right)^2 \tag{3}$$

where d_c is the tube diameter. Hence, this simplified work done model gives:

$$E_c = \frac{p_{CJ} u_{CJ} \pi d_c^3}{8 a_{CJ}} \tag{4}$$

It is thus suggested by Eq. 4 that the critical tube diameter and critical initiation energy can be directly linked with each other by this work done model. With the knowledge of experimentally measured and theoretically predicted critical tube diameter data introduced in the previous section, critical initiation energy can be approximated and compared with the experimental measurement. From the comparison between theoretical prediction and experimentally measured data which is shown in Fig. 6, it is found that the theoretical prediction can estimate the critical energy at each initial pressure with very reasonable accuracy.

Fig. 7 shows the variation of experimental and predicted critical energies versus equivalence ratio for C_2H_2/N_2O mixtures at the initial pressure of 100 kPa. Both the experimental data and the theoretical prediction curves indicate that the critical initiation energy along with its equivalence ratio φ is in the form of typical "U" shape, and the minimum of the critical initiation energy appears around $\varphi = 2.5$. This behavior is in good agreement with the induction zone length variation curve obtained from chemical kinetics calculation, which is shown in Fig. 8. The explosive sensitivity characterized by the direct initiation energy also agrees with the critical tube diameter results, which both show that C_2H_2/N_2O mixture is most sensitive around $\varphi = 2.5$.

To look at the dilution effect, Fig. 9 shows the critical energy for C_2H_2/N_2O mixtures diluted with different amounts of inert argon. As seen from Fig. 9 that with an increase of the amount of argon dilution, the critical initiation energy increases consequently; In other words, with more argon dilution, the mixtures tend to be less sensitive to detonation. As shown in Fig. 10 the variation of induction length as a function of amount of Ar dilution, by increasing the amount of argon dilution, the induction zone length increases, which can also explain qualitatively the increase of critical initiation energy.

3.3 Critical energy comparison between $C_2H_2/N_2O/Ar$ and $H_2/N_2O/Ar$ mixtures

The critical energies of direct detonation initiation for stoichiometric C_2H_2/N_2O and H_2/N_2O mixtures as a function of initial pressure are compared in Fig. 11. By comparing the results for stoichiometric C_2H_2/N_2O and H_2/N_2O mixtures at the same initial pressure, it is clear that the critical energies for H_2/N_2O are always higher than those of C_2H_2/N_2O at the range of initial pressures considered in this study. Fig. 12 shows the results of induction length scale analysis; As can be seen that the induction length of H_2/N_2O is around 4 times larger than that of C_2H_2/N_2O mixture. Equivalently, the larger induction length scale results in the bigger critical energy required for direct initiation of a detonation.

The experimentally measured critical initiation energies for C_2H_2/N_2O and H_2/N_2O mixtures at atmospheric pressure with the variation of equivalence ratio are shown in Fig. 13. Both curves of critical energy variation with equivalence ratio for C_2H_2/N_2O and H_2/N_2O mixtures are again described by the typical “U” shape behavior. However, the minimum critical energy of H_2/N_2O is around $\varphi = 0.8$, and for the C_2H_2/N_2O mixtures, the minimum critical energy occurs around $\varphi = 2.5$. It also appears that the C_2H_2/N_2O is more sensitive than H_2/N_2O at the rich side. This scenario is very similar from the chemical kinetic point-of-view demonstrated by the induction length variation with equivalence ratio for both mixtures, which are shown in Fig. 8 and Fig. 14. It can be seen that the minimum critical energy always occurs at the composition where induction length has the minimum value.

The critical initiation energy results for stoichiometric C_2H_2/N_2O and H_2/N_2O with different amounts of argon dilution mixtures are shown in Fig. 15. One can note that with an increase of argon dilution, the critical energy for both mixtures increases. However, it increases only very slightly for $C_2H_2/N_2O/Ar$ mixture, yet for $H_2/N_2O/Ar$ mixture the increase of critical energy appears much steeper. In addition, the results of induction length analysis are shown in Fig. 16, which indicate that for the H_2/N_2O mixture, the induction zone length scale is always bigger than C_2H_2/N_2O when diluted with the same amount of argon.

One interesting observation is that although the ZND induction lengths for both mixtures do not vary significantly with increasing argon dilution, one can notice in Fig. 15 that there appears a fast increase in critical energy for H_2/N_2O mixtures with dilution above 30% and for C_2H_2/N_2O mixtures diluted with more than 50%. This fast increase in the critical energy could perhaps be related to the dynamic effect instead of the chemical effect [25, 26, 43]. It is known that by increasing the argon dilution, the detonation wave becomes more stable in the sense that the reaction zone structure is more regular with weaker transverse waves [44], and the dynamic change in the regularity of the detonation structure is known to have an effect on the propagation, limits and initiation of a detonation wave [45]. Previous studies proposed that the stability of the detonation wave can be characterized by a stability parameter χ, calculated by the effective activation energy of the induction zone multiplied by the ratio of induction to exothermic heat release length [43, 46]. As shown in our previous work [25], stable or regular mixtures characterized by small instability parameter χ tend to be less sensitive to detonation initiation. Looking at Fig. 17 which shows the stability parameter χ for both mixtures as a function of the degree of argon dilution, by increasing the argon dilution the stability parameters χ for both mixtures decrease and the detonation shall become more stable and therefore, the increase in critical energy as shown in Fig. 15 can be explained from this detonation instability consideration. Furthermore, the rate of decrease in χ for H_2/N_2O mixtures by increasing the argon dilution appears to be faster than that of C_2H_2/N_2O, and hence, it also explains why the onset of the fast increase in critical energy for H_2/N_2O mixtures is earlier at about 30%.

From the critical energy comparison between $C_2H_2/N_2O/Ar$ and $H_2/N_2O/Ar$ mixtures, all results suggest that $C_2H_2/N_2O/Ar$ is more detonation sensitive than $H_2/N_2O/Ar$ at the same initial conditions, which can also be proven from the ZND analysis that the induction length scale for $C_2H_2/N_2O/Ar$ is always smaller than that of $H_2/N_2O/Ar$ mixture.

3.4 Critical energy comparison between $C_2H_2/N_2O/Ar$ and $C_2H_2/O_2/Ar$ mixtures

To study the effect of the oxidizer on the critical initiation energy, a series of experiments using mixtures of $C_2H_2/O_2/Ar$ at the similar initial conditions as those with $C_2H_2/N_2O/Ar$ mixtures were also performed in order to make comparison of their critical energies and further investigate chemical kinetic effects in using different oxidants.

Figure 18 shows the critical energy of direct detonation initiation for stoichiometric C_2H_2/N_2O and C_2H_2/O_2 mixtures as a function of the initial pressure. Due to the different order of magnitude of the detonation sensitivity of these mixtures, and to guarantee the accuracy of the measurement, the critical energies of both mixtures were measured at the different range of initial pressure. Nevertheless, from the tendency of the curve fit with experimental data, it is readily seen that the critical energy C_2H_2/N_2O mixture is around 2 orders of magnitude bigger than that of C_2H_2/O_2 if the same initial pressure is considered. Once again, from the aspect of induction length analysis, which is shown in Fig. 19, it is observed that the ZND induction length scale for C_2H_2/N_2O is around 3 times bigger than that of C_2H_2/O_2 when at the low pressure, and about the ratio is about 10 as the pressure increases above 100 kPa. It is also interesting to notice that the ratio between the two critical energies of C_2H_2/N_2O and C_2H_2/O_2 mixtures found in Fig. 18 is of the order of 400. Using the ZND induction length as the characteristic length scale, from dimensional consideration the initiation energy should scale according to $E_c \sim \Delta^3$ and hence, the ratio of the ZND induction length between these two mixtures should be approximately of the order of 7. This agree well with the results shown in Fig. 19 which shows on average a ratio of 6 over the initial pressure range considered in this study. A discrepancy is expected since it is known that the scaling $E_c \sim \Delta^3$ is not appropriate for unstable detonations with irregular reaction zone structures and the energy formula in general depends also on the CJ detonation velocity, density ρ_0, specific heat ratio γ, cell size λ, etc., $E_c \sim \rho_0 D_{CJ}^2 \lambda_{CJ}^3$ [47]. These parameters vary also between $C_2H_2/N_2O/Ar$ and $C_2H_2/O_2/Ar$ mixtures.

The critical initiation energies for C_2H_2/N_2O and C_2H_2/O_2 mixtures at different equivalence ratios were also experimentally measured to observe whether the minima move by using different oxidizers and results are shown in Fig. 20. It should be noted that the initial pressure does not change the minimum critical energy behavior with the variation of equivalence ratio, and again due to the high detonation sensitivity of C_2H_2/O_2 mixtures and experimental limitations, the initial pressure of C_2H_2/O_2 of 10 kPa is used instead in this study. It can be seen from Fig. 21 that the minimum critical energies locate at about $\varphi = 2.5$ for both mixtures. If one looks at the induction zone length variation with equivalence ratio, the induction zone length also arrives at the minimum value around $\varphi = 2.5$ for both mixtures under the atmospheric pressure. The result shows that the minimum critical energy behavior is in agreement with that of induction zone length.

The last part of this study aims to look at the critical initiation energy for stoichiometric

C_2H_2/N_2O and C_2H_2/O_2 mixtures diluted with different amounts of argon and the results are shown in Fig. 22. For the undiluted case and 22% argon dilution in C_2H_2/O_2 mixtures, the critical energies were obtained by the theoretical predictions which are based on the experimental measured cell sizes data combined with the model presented earlier in this paper and the classical relationship $d_c = 13\lambda$. The cell size for the undiluted and 22% argon diluted C_2H_2/O_2 mixtures are extracted from the CALTECH detonation database [48] and the dissertation by Radulescu [43], respectively. The experimental data curve fits show that with increasing amount of argon dilution, the critical energies increase for both mixtures. However, the critical energy for $C_2H_2/N_2O/Ar$ mixture is always 2 orders of magnitude larger than that of $C_2H_2/O_2/Ar$ mixture with the same amount of argon dilution. Fig. 23 shows the induction length variation for these mixtures; it is apparent that the induction length for $C_2H_2/N_2O/Ar$ is around one order of magnitude bigger than that of $C_2H_2/O_2/Ar$ mixture.

From the critical energy comparison between $C_2H_2/N_2O/Ar$ and $C_2H_2/O_2/Ar$ mixtures, it can be found that the mixture tends to be less detonation sensitive by using nitrous oxide as oxidizer than using oxygen, thus more energy is needed to achieve a successful direct initiation. The experiment results also indicate that the oxidizer does not change the overall critical energy behavior and the location of its minimum.

4. Concluding remarks

In this study, detonation critical tube diameters were measured for $C_2H_2/N_2O/Ar$ mixtures at various initial conditions (i.e., $\varphi = 0.625 - 2.5$ and argon dilution up to 50%, respectively). Using chemical kinetic calculation with Konnov mechanism (Release 0.3) and present experimental data, a simple correlation for the detonation critical tube diameter of $C_2H_2/N_2O/Ar$ mixtures with the ZND induction zone length scale, i.e., $d_c = 594.8\varphi^{0.623}(1 - X_{Ar})^{0.2176}(p/p^{o})^{-0.0246}\Delta_I$ is developed valid for the stoichiometric mixture at different initial pressures ranging from 50 to 130 kPa, equivalence ratios from 0.625 - 2.5 and stoichiometric mixtures with the maximum percentage of Ar dilution up to 50% at atmospheric pressure. The critical energy for direct blast initiation can also be predicted by combining this correlation function with a work done model, and the results show reasonable accuracy by the comparison with those measured experimentally.

The critical energy results for direct initiation of detonation in $C_2H_2/N_2O/Ar$ mixtures are compared with those in $H_2/N_2O/Ar$ mixtures. The results indicate $C_2H_2/N_2O/Ar$ is more sensitive than $H_2/N_2O/Ar$ at the same initial conditions. The effect of the oxidizer on the detonation sensitivity is also investigated by comparing the critical energy between $C_2H_2/N_2O/Ar$ and $C_2H_2/O_2/Ar$ mixtures. The results show that the mixture tends to be less detonation sensitive by using nitrous oxide as oxidizer than oxygen if the same initial condition is considered, thus higher initiation energy is required to achieve direct initiation of a spherical detonation in $C_2H_2/N_2O/Ar$ than in $C_2H_2/O_2/Ar$ mixtures. To explain qualitatively these variations of critical initiation energy and critical tube diameter observed in the experiments, ZND induction length analysis is also performed. Such analysis, from chemical kinetic consideration, has proven to provide some insights on the qualitative trends of detonation dynamic parameters with different initial conditions. In all cases, the critical initiation energy behavior agrees accordingly with the variation of the ZND induction length.

Acknowledgments

BZ thanks the Chinese Scholarship Council (CSC) for the granting of a fellowship for research at McGill University. This work is supported by the Natural Sciences and Engineering Research Council of Canada (NSERC). Detailed suggestions and helpful comments by the reviewers are gratefully acknowledged.

Reference

[1] E. Eger, Nitrous Oxide, Edward Arnold Ltd, New York, 1985.

[2] G.P. Sutton, O. Biblarz, Rocket Propulsion Elements, 7th ed., Wiley-Interscience, 2000.

[3] G.W. Rhodes, Investigation of Decomposition Characteristics of Gaseous and Liquid Nitrous Oxide, AD-784 802, AFWL-TR-73-299, Air Force Weapons Laboratory, Kirtland AFB, NM 87117, July 1974.

[4] C. Merrill, Nitrous Oxide Explosive Hazards, Air Force research laboratory, AFRL-RZ-ED-TP-2008-184.

[5] U. Pfahl, M. Ross, J.E. Shepherd, Combust Flame, 123 (2000) 140-58.

[6] R. Akbar, M. Kaneshige, E. Schultz, J.E. Shepherd, Detonations in H_2-N_2O-CH_4-NH_3-O_2-N_2 Mixtures, GALCIT Technical Report FM-97-3, 1997.

[7] K. Cashdollar, M. Hertzberg, I. Zlochower, C. Lucci, G. Grenn, R. Thomas, Laboratory Flammability Studies of Mixtures of Hydrogen, Nitrous Oxide, and Air, Technical Report WHC-SDWMES-219. Pittsbrugh Research Center, 1992.

[8] R. Mével, S. Javoy, F. Lafosse, N. Chaumeix, G. Dupré, C.E. Paillard, Proc. Combust. Inst. 32 (2009) 359-366.

[9] R. Mével, F. Lafosse, N. Chaumeix, G. Dupré, C.E. Paillard, Int. J. Hydrogen Energy 34(21) (2009) 9007-9018.

[10] R. Mével, F. Lafosse, L. Catoire, N. Chaumeix, G. Dupré, C.E. Paillard, Combust. Sci. Tech. 180 (2008) 1858-1875.

[11] S.P.M. Bane, R. Mével, S.A. Coronel, J.E. Shepherd, Flame burning speeds and combustion characteristics of undiluted and nitrogen-diluted hydrogen nitrous oxide mixtures, Int. Hydrogen Energy, (2011) In press.

[12] M. Ross, J.E. Shepherd, Lean Combustion Characteristics of Hydrogen-Nitrous Oxide-Ammonia Mixtures in Air, GALCIT Technical Report FM-96-4, 1996.

[13] M. Kaneshige, E. Schultz, U Pfahl, J.E. Shepherd. R. Akbar, Proc. 22nd Int. Sym. Shock Waves, (2000) 251-256.

[14] M.S. Gerber, Legend and Legacy: Fifty Years of Defense Production at the Hanford Site, Tech. Rep. WHC-MRe0293- Rev.2. Westinghouse Hanford Co., 1992.

[15] N.D. Lichtenstein, Nat Resour J. 44 (2004) 809-839.

[16] L.A. Mahoney, J.L. Huckaby, S.A. Bryan, G.D. Johnson, Overview of the Flammability of Gases Generated in Hanford Waste Tanks, Tech. Rep. PNNL-13269. Richland, Wash: Pac Northwest Natl Lab, 2000.

[17] W.R. Moomaw, AMBIO: A Journal of the Human Environment 31 (2002) 184-189.

[18] H. Matsui and J.H.S. Lee, Proc. Combust. Inst. 17 (1978) 1269.

[19] J. H. Lee, Ann. Rev. Fluid. Mech. 16 (1984) 311-336.

[20] J.C. Libouton, A. Jacques, P.J. Van Tiggelen, Proc. Colloque Int. Berthelot - Vieille-Mallard-LeChatelier, Bordeaux, France, 2 (1981) 437 -444.

[21] F. Pintgen, J.M. Austin, J.E. Shepherd, Detonation Front Structure: Variety and Characterization, in Confined Detonations and Pulse Detonation Engines, Roy, G.D., Frolov, S.M., Santoro, R.J., Tsyganov, S.A.(eds). Torus Press, Moscow, 2003.

[22] B. Zhang, H.D. Ng, J.H.S. Lee, Direct measurement and relationship between critical tube diameter and critical energy for direct detonation initiation. 23rd Int. Colloquium on the Dynamics of Explosions and Reactive Systems, Irvine, US, July 24-29, 2011. Also submitted to J. Loss Prev. Proc. Ind. (Sept. 2011).

[23] R. Knystautas, J.H.S. Lee, Combust. Flame, 27 (1976) 221-228.

[24] V. Kamenskihs, H.D. Ng, J.H.S. Lee, Combust. Flame, 157 (9) (2010) 1795-1799.

[25] B. Zhang, H.D. Ng, R. Mével, J.H.S. Lee, Int. J. Hydrogen Energy, 36 (2011) 5707-5716.

[26] B. Zhang, V. Kamenskihs, H.D. Ng, J.H.S. Lee, Proc. Combust. Inst., 33 (2) (2011) 2265-2271.

[27] B. Zhang, H.D. Ng, J.H.S. Lee, Shock Waves, DOI: 10.1007/s00193-011-0351-x.

[28] B. Zhang, H.D. Ng, J.H.S. Lee, Shock Waves, 22(1) (2012) 1-7.

[29] T. Lu, C.K. Law, Y. Ju, J. Propulsion Power, 19 (5) (2003) 901-907.

[30] R.J. Kee, F.M. Rupley, J.A. Miller, Sandia National Laboratories report SAND89-8009, 1989.

[31] A.A. Konnov, Detailed reaction mechanism for small hydrocarbons combustion. Release 0.3, 1997, http://homepages.vub.ac.be/~akonnov/

[32] Y. Tan, P. Dagaut, M. Cathonnet, J.C. Boettner, Combust. Sci. Tech, 102 (1994) 21-55.

[33] J. Card, D. Rival, G.. Ciccarelli, Shock Waves, 14 (3) (2005) 167-173.

[34] J.M. Austin, F. Pintgen, J.E. Shepherd. Proc. Combust. Inst.30 (2) (2005) 1849–1857.

[35] L. Massa, J.M. Austin, T.L. Jackson, J. Fluid Mech. 586 (2007) 205-248.

[36] E. Schultz, J.E. Shepherd, Validation of Detailed Reaction Mechanisms for Detonation Simulation, GALCIT Technical Report FM99-5, 2000.

[37] J.A. Miller, C.T. Bowman, Prog. Energy Combust. Sci., 15 (1989) 287-338.

[38] M.A. Mueller, R.A. Yetter, F.L. Dryer. Int. J. Chem. Kinet., 32 (2000) 317–339

[39] S. Laberge, R. Knystautas, J.H.S. Lee, Prog. Astro. Aero., 153 (1993) 380-396.

[40] D. Desbordes, Prog. Astro. Aero., 11 (1988) 170-185.

[41] I. Sochet, T. Lamy, J. Brossard, C. Vaglio, R. Cayzac, Shock Waves 9 (1999) 113-123.

[42] A.A. Vasil'ev, Combust. Expl. Shock Waves, 34(4) (1998) 433-437.

[43] M.I. Radulescu, The Propagation and Failure Mechanism of Gaseous Detonations: Experiments in Porous-Walled Tubes. Ph.D. thesis, McGill University, Canada, 2003.

[44] M.I. Radulescu, H.D. Ng, J.H.S. Lee, B. Varatharajan, Proc. Combust. Inst. 29 (2002) 2825–2831.

[45] J.H.S. Lee, *The Detonation Phenomenon*. Cambridge University Press, 2008.

[46] H.D. Ng, M.I. Radulescu, A.J. Higgins, N. Nikiforakis, J.H.S. Lee, Combust. Theory Model. 9 (3) (2005) 385–401.

[47] D. Desbordes, C. Guerraud, L. Hamada, H.N. Presles, Prog. Astronaut. Aeronaut. 153 (1993) 347-359.

[48] M. Kaneshige, J.E. Shepherd, *Detonation Database*. GALCIT report FM97-8, California Institute of Technology, Pasadena, CA, 1997.

Table

Table 1. Initial conditions used in the critical tube diameter experiment for C_2H_2/N_2O mixture

Table 2. Initial conditions used in the direct initiation experiment

Equivalence Ratio (φ)	Initial Pressure (kPa)	Argon Dilution (%)
0.625-2.5	38-200	0-50

Table 1.

Mixtures	Initial Pressure (kPa)	Equivalence Ratio (φ)	Argon Dilution (%)
$C_2H_2/N_2O/Ar$	50-200	0.56-3.0	0-50
$H_2/N_2O/Ar$	70-200	0.5-1.2	0-30
$C_2H_2/O_2/Ar$	5-25	0.625-4	0-70

Table 2.

Figure captions

Fig. 1. Experimental setup for the critical tube diameter experiment

Fig. 2. Arrival time trace showing a planar detonation successfully emerged from the small steel tube *d* = 19.1 mm into the large spherical chamber for the stoichiometric C_2H_2-$5N_2O$ mixture at an initial pressure of 58 kPa

Fig. 3. Experimental setup for the direct blast initiation experiment

Fig. 4. The variation of tube diameter versus initial pressure at various compositions for C_2H_2/N_2O mixtures

Fig. 5. The variation of tube diameter versus initial pressure at different amount of argon dilution for C_2H_2/N_2O mixtures

Fig. 6. Critical energy as a function of initial pressure from experimental measurement and theoretical prediction for stoichiometric C_2H_2/N_2O mixture

Fig. 7. Critical energy as a function of equivalence ratio from experimental measurement and theoretical prediction for C_2H_2/N_2O mixture at p_0 = 100 kPa

Fig. 8. Induction length as a function of equivalence ratio for C_2H_2/N_2O mixture at p_0 = 100 kPa

Fig. 9. Critical energy as a function of argon dilution from experimental measurement and theoretical prediction for stoichiometric C_2H_2/N_2O mixture at p_0 = 100 kPa

Fig. 10. Induction length scale as a function of argon dilution for stoichiometric C_2H_2/N_2O mixture at p_0 = 100 kPa

Fig. 11. Critical energy as a function of initial pressure for stoichiometric C_2H_2/N_2O and H_2/N_2O mixtures

Fig. 12. Induction length as a function of initial pressure for stoichiometric C_2H_2/N_2O and H_2/N_2O mixtures

Fig. 13. Critical energy as a function of equivalence ratio for a) H_2/N_2O and b) C_2H_2/N_2O mixtures at p_0 =100 kPa

Fig. 14. Induction length as a function of equivalence ratio for H_2/N_2O mixture at p_0 = 100 kPa

Fig. 15. Critical energy as a function of % argon dilution for stoichiometric H_2/N_2O and C_2H_2/N_2O mixtures at the initial pressure of p_0 = 100 kPa

Fig. 16. Induction length as a function of % argon dilution for stoichiometric H_2/N_2O and C_2H_2/N_2O mixtures at p_0 = 100 kPa

Fig. 17. Stability parameter χ as a function of the degree of argon dilution for stoichiometric H_2/N_2O and C_2H_2/N_2O mixtures

Fig. 18. Critical energy as a function of initial pressure for stoichiometric C_2H_2/N_2O and C_2H_2/O_2 mixtures

Fig. 19. Induction length as a function of initial pressure for stoichiometric C_2H_2/N_2O and C_2H_2/O_2 mixtures

Fig. 20. Critical energy as a function of equivalence ratio for C_2H_2/N_2O and C_2H_2/O_2 mixtures

Fig. 21. Induction length as a function of equivalence ratio for C_2H_2/N_2O and C_2H_2/O_2 mixtures at $p_0 = 100$ kPa

Fig. 22. Critical energy as a function of % argon dilution for stoichiometric C_2H_2/N_2O and C_2H_2/O_2 mixtures

Fig. 23. Induction length as a function of % argon dilution for stoichiometric C_2H_2/N_2O and C_2H_2/O_2 mixtures

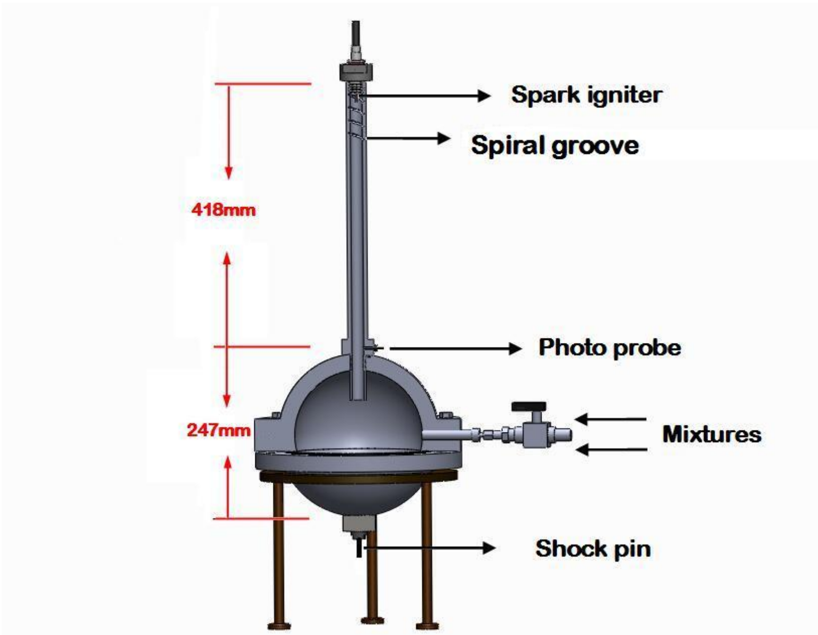
Spark igniter
Spiral groove
418mm
Photo probe
247mm
Mixtures
Shock pin

Fig. 1

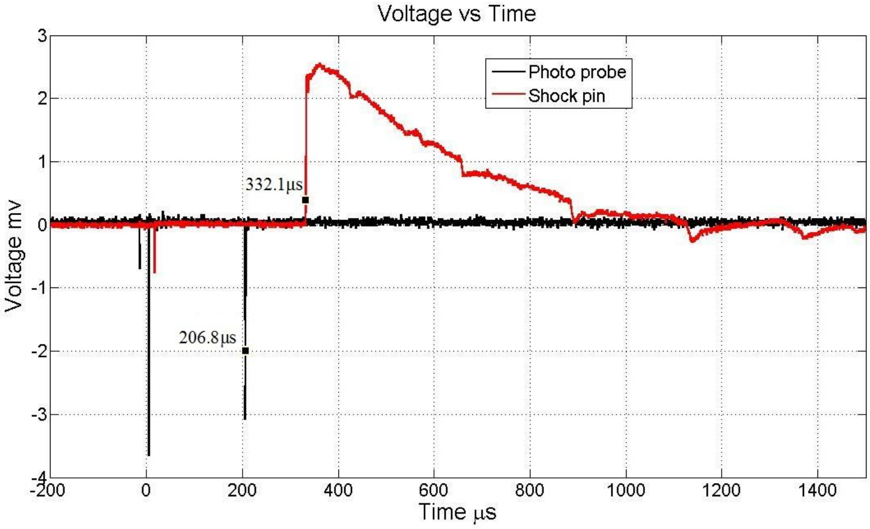
Voltage vs Time
Photo probe
Shock pin
332.1μs
206.8μs
Voltage mv
Time μs
3
2
1
0
-1
-2
-3
-4
-200
0
200
400
600
800
1000
1200
1400

Fig. 2

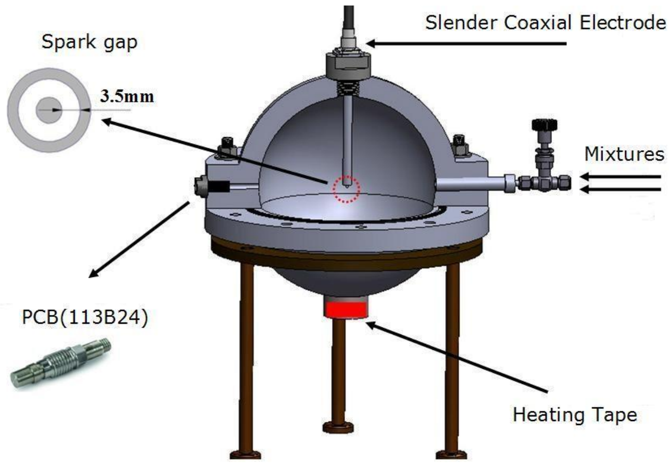
Spark gap
3.5mm
Slender Coaxial Electrode
Mixtures
PCB(113B24)
Heating Tape

Fig. 3

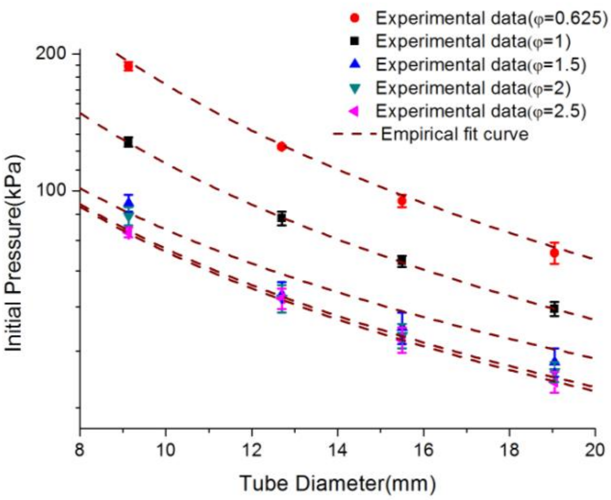

Experimental data(φ=0.625)
Experimental data(φ=1)
Experimental data(φ=1.5)
Experimental data(φ=2)
Experimental data(φ=2.5)
Empirical fit curve
200
100
Initial Pressure(kPa)
8
10
12
14
16
18
20
Tube Diameter(mm)

Fig. 4

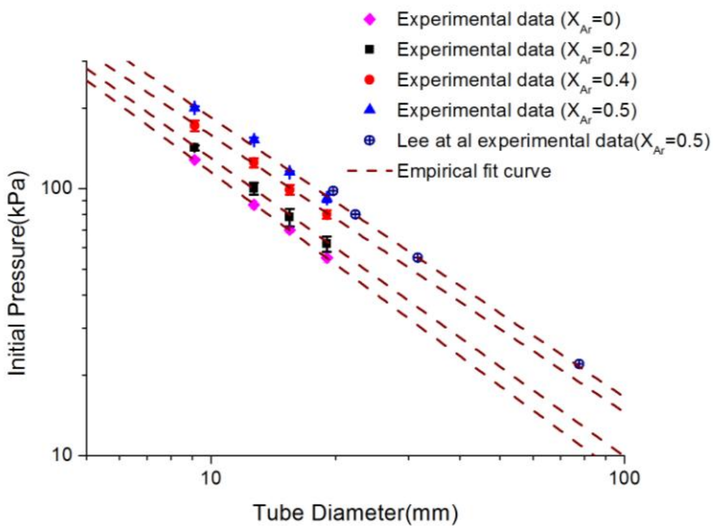
Experimental data (X_{Ar}=0)
Experimental data (X_{Ar}=0.2)
Experimental data (X_{Ar}=0.4)
Experimental data (X_{Ar}=0.5)
Lee at al experimental data(X_{Ar}=0.5)
Empirical fit curve
Initial Pressure(kPa)
100
10
10
100
Tube Diameter(mm)

Fig. 5

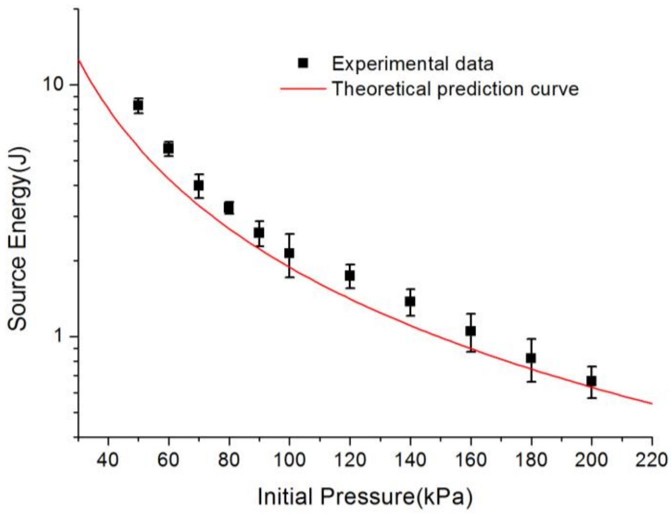
Experimental data
Theoretical prediction curve
Source Energy(J)
10
1
40
60
80
100
120
140
160
180
200
220
Initial Pressure(kPa)

Fig. 6

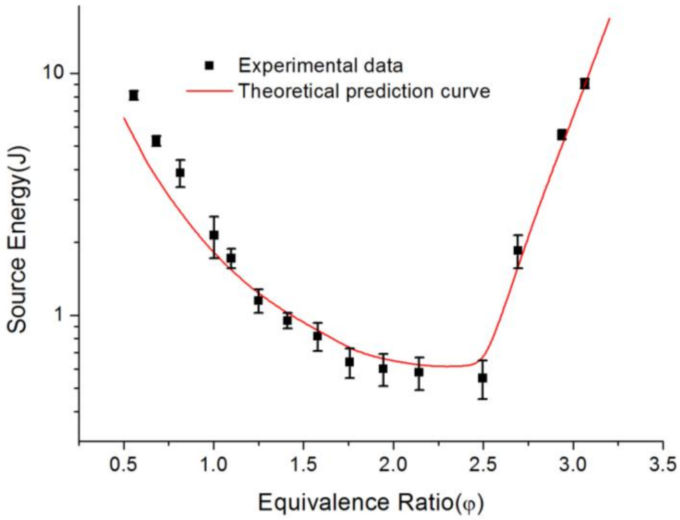

Experimental data
Theoretical prediction curve
Source Energy(J)
10
1
0.5
1.0
1.5
2.0
2.5
3.0
3.5
Equivalence Ratio(φ)

Fig. 7

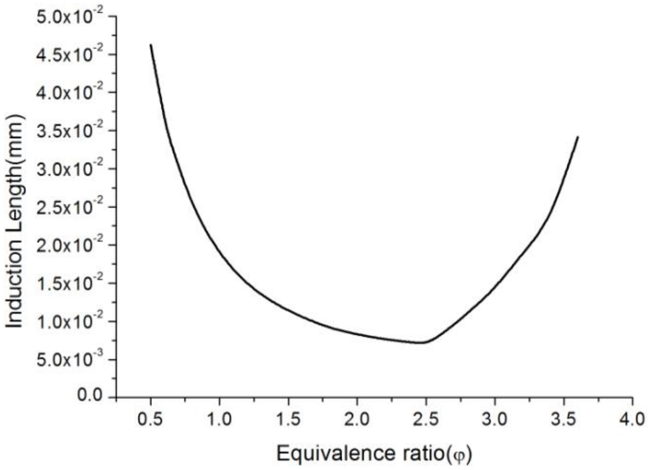
Induction Length(mm)
5.0x10^{-2}
4.5x10^{-2}
4.0x10^{-2}
3.5x10^{-2}
3.0x10^{-2}
2.5x10^{-2}
2.0x10^{-2}
1.5x10^{-2}
1.0x10^{-2}
5.0x10^{-3}
0.0
0.5
1.0
1.5
2.0
2.5
3.0
3.5
4.0
Equivalence ratio(φ)

Fig. 8

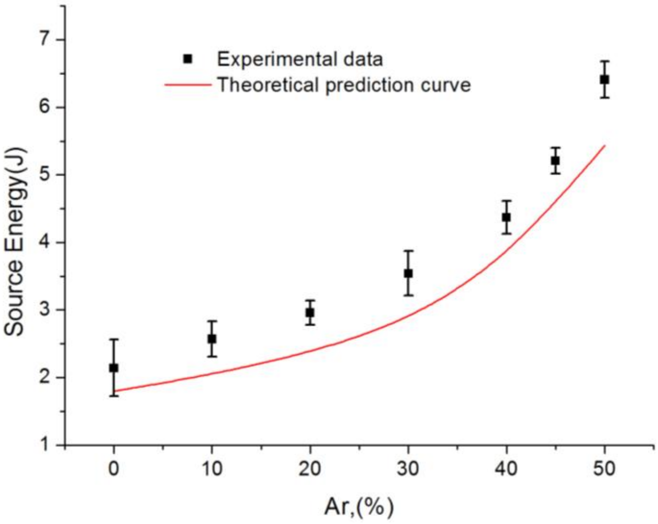
Experimental data
Theoretical prediction curve
Source Energy(J)
Ar,(%)
1
2
3
4
5
6
7
0
10
20
30
40
50

Fig. 9

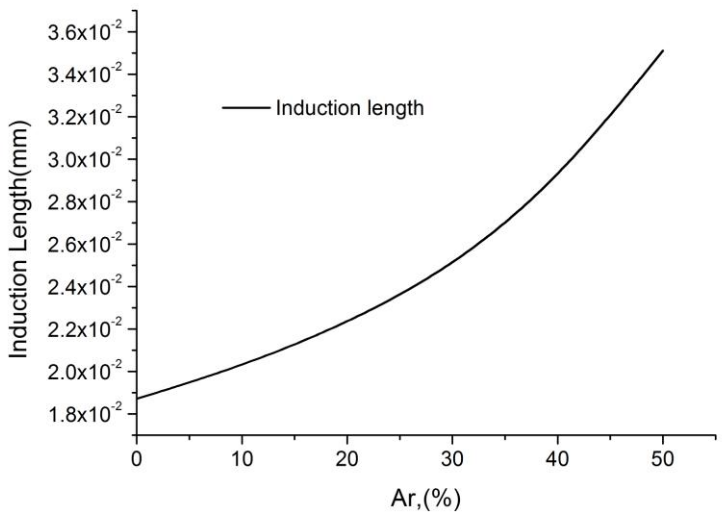
Induction length
Induction Length(mm)
3.6x10-2
3.4x10-2
3.2x10-2
3.0x10-2
2.8x10-2
2.6x10-2
2.4x10-2
2.2x10-2
2.0x10-2
1.8x10-2
0
10
20
30
40
50
Ar,(%)

Fig. 10

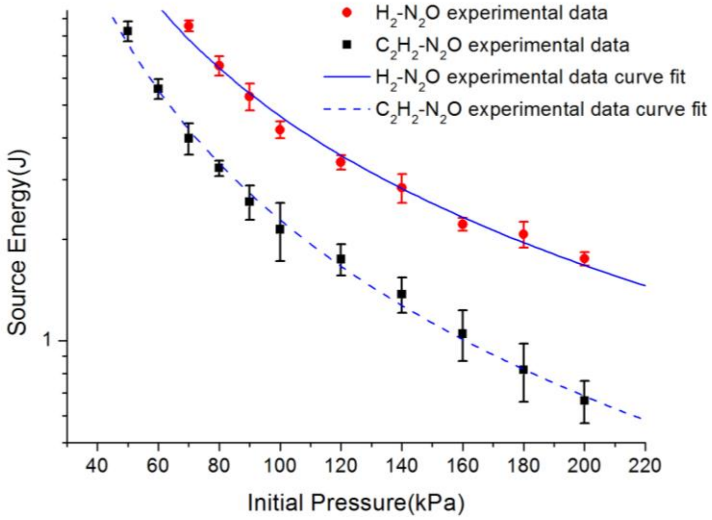

H_2-N_2O experimental data
C_2H_2-N_2O experimental data
H_2-N_2O experimental data curve fit
C_2H_2-N_2O experimental data curve fit
Source Energy(J)
1
40
60
80
100
120
140
160
180
200
220
Initial Pressure(kPa)

Fig. 11

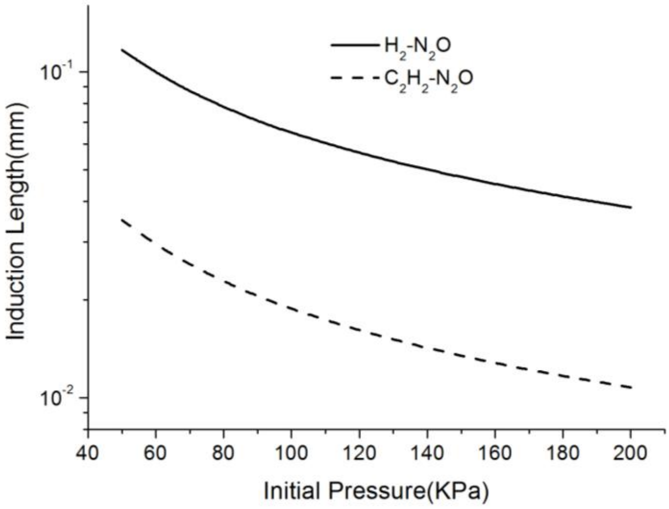

H_2-N_2O
C_2H_2-N_2O
Induction Length(mm)
10^{-1}
10^{-2}
40 60 80 100 120 140 160 180 200
Initial Pressure(KPa)

Fig. 12

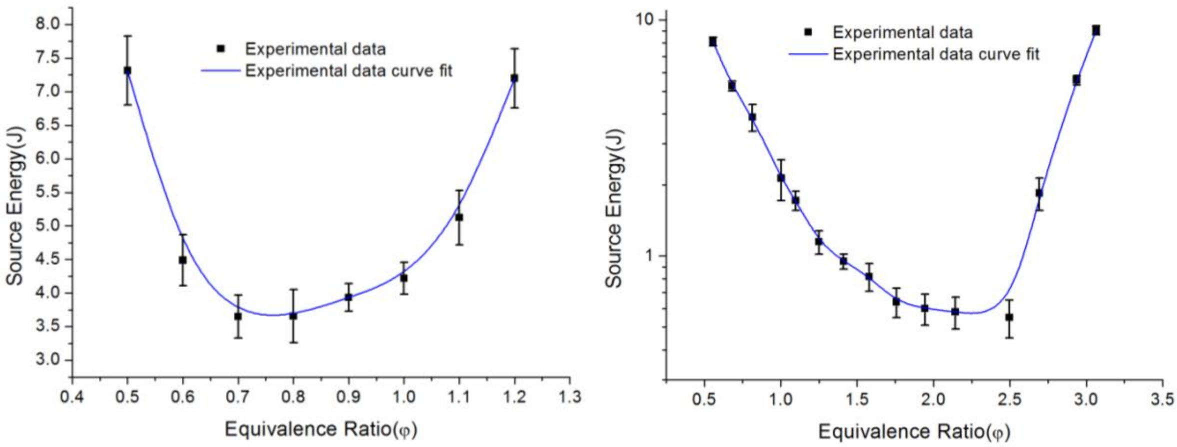
Source Energy(J)
Equivalence Ratio(φ)
Experimental data
Experimental data curve fit
8.0
7.5
7.0
6.5
6.0
5.5
5.0
4.5
4.0
3.5
3.0
0.4
0.5
0.6
0.7
0.8
0.9
1.0
1.1
1.2
1.3
Source Energy(J)
Equivalence Ratio(φ)
Experimental data
Experimental data curve fit
10
1
0.5
1.0
1.5
2.0
2.5
3.0
3.5

(a) **(b)**

Fig. 13

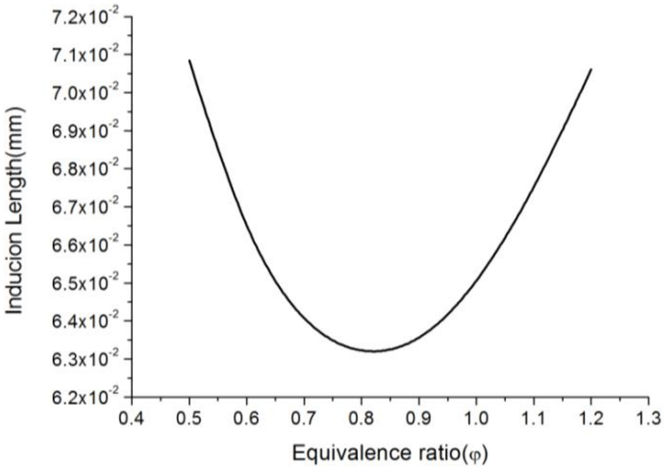

7.2x10^-2
7.1x10^-2
7.0x10^-2
6.9x10^-2
6.8x10^-2
6.7x10^-2
6.6x10^-2
6.5x10^-2
6.4x10^-2
6.3x10^-2
6.2x10^-2
Inducion Length(mm)
0.4
0.5
0.6
0.7
0.8
0.9
1.0
1.1
1.2
1.3
Equivalence ratio(φ)

Fig. 14

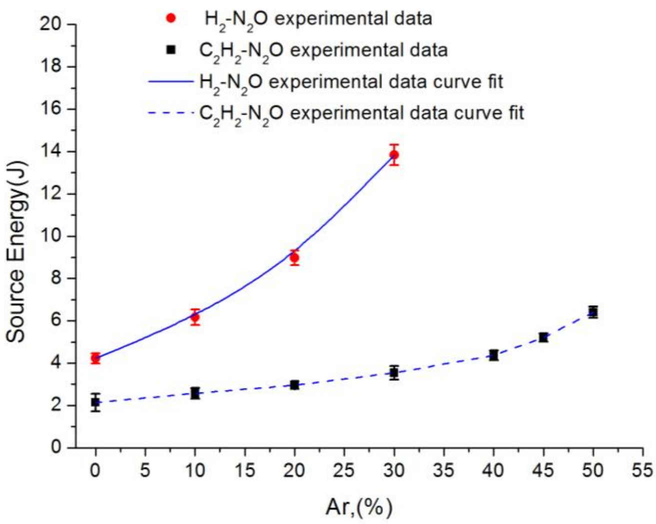
H2-N2O experimental data
C2H2-N2O experimental data
H2-N2O experimental data curve fit
C2H2-N2O experimental data curve fit
Source Energy(J)
Ar,(%)
0
2
4
6
8
10
12
14
16
18
20
0
5
10
15
20
25
30
35
40
45
50
55

Fig. 15

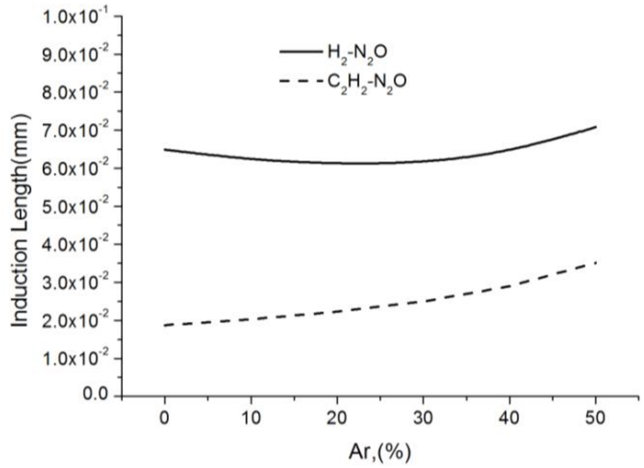
H2-N2O
C2H2-N2O
Induction Length(mm)
1.0x10-1
9.0x10-2
8.0x10-2
7.0x10-2
6.0x10-2
5.0x10-2
4.0x10-2
3.0x10-2
2.0x10-2
1.0x10-2
0.0
0
10
20
30
40
50
Ar,(%)

Fig. 16

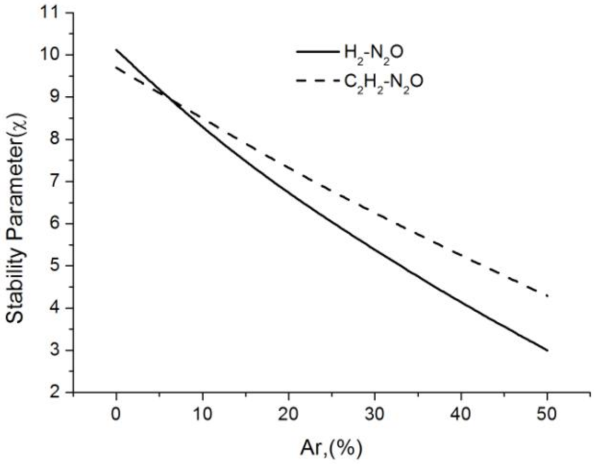

11
10
9
8
7
6
5
4
3
2
Stability Parameter(χ)
0
10
20
30
40
50
Ar,(%)
H2-N2O
C2H2-N2O

Fig. 17

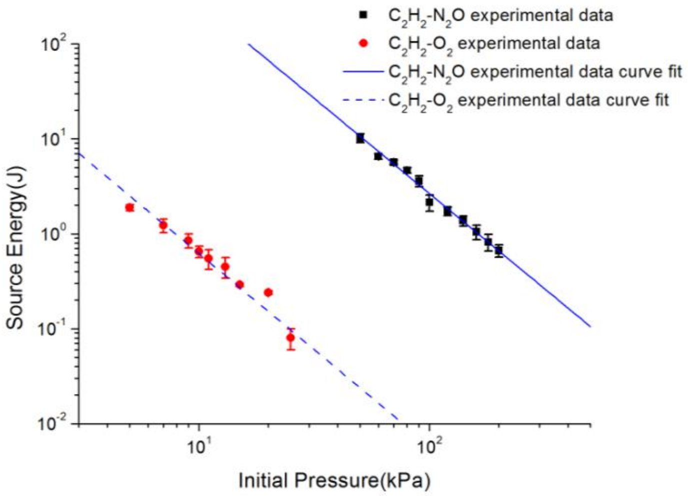

C2H2-N2O experimental data
C2H2-O2 experimental data
C2H2-N2O experimental data curve fit
C2H2-O2 experimental data curve fit
Source Energy(J)
Initial Pressure(kPa)

Fig. 18

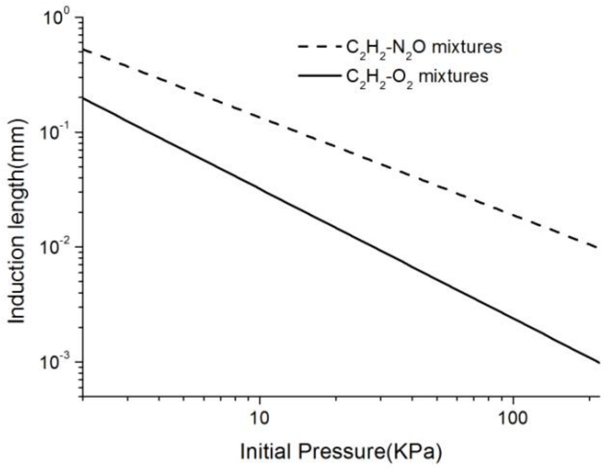

10^0
10^{-1}
10^{-2}
10^{-3}
Induction length(mm)
C_2H_2-N_2O mixtures
C_2H_2-O_2 mixtures
10
100
Initial Pressure(KPa)

Fig. 19

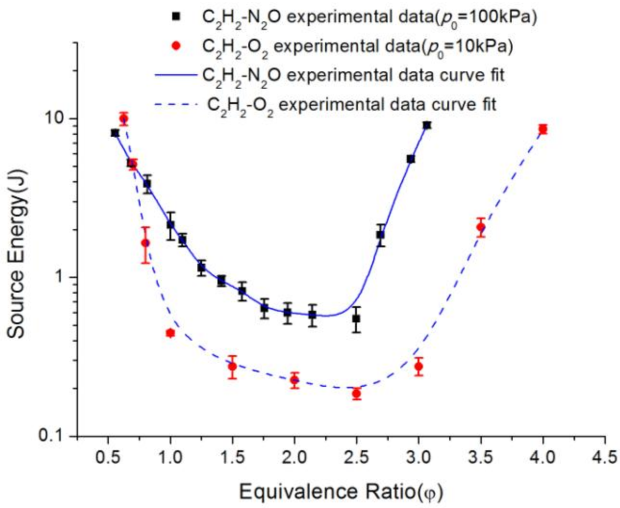

C2H2-N2O experimental data(p0=100kPa)
C2H2-O2 experimental data(p0=10kPa)
C2H2-N2O experimental data curve fit
C2H2-O2 experimental data curve fit
Source Energy(J)
10
1
0.1
0.5
1.0
1.5
2.0
2.5
3.0
3.5
4.0
4.5
Equivalence Ratio(φ)

Fig. 20

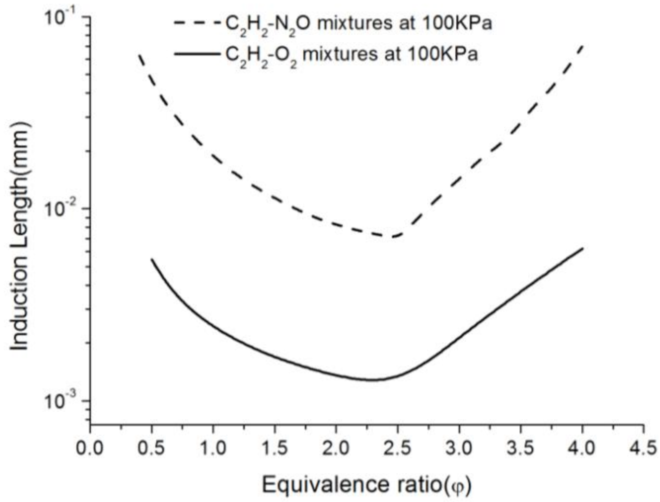

C2H2-N2O mixtures at 100KPa
C2H2-O2 mixtures at 100KPa
Induction Length(mm)
10-1
10-2
10-3
0.0
0.5
1.0
1.5
2.0
2.5
3.0
3.5
4.0
4.5
Equivalence ratio(φ)

Fig. 21

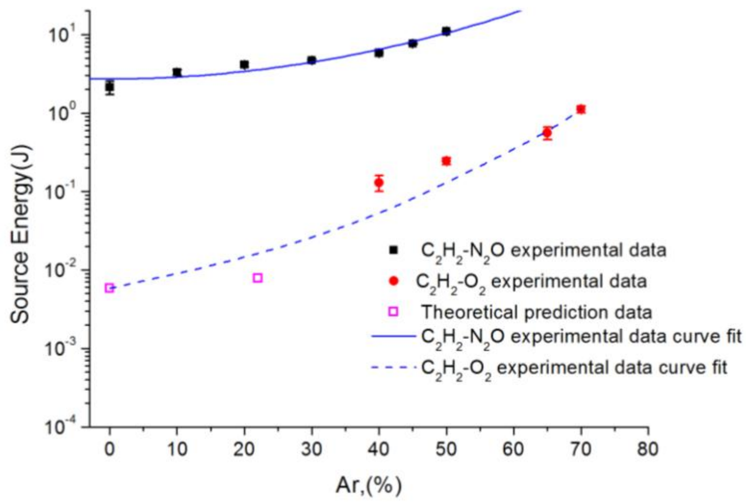
Source Energy(J)
Ar,(%)
C_2H_2-N_2O experimental data
C_2H_2-O_2 experimental data
Theoretical prediction data
C_2H_2-N_2O experimental data curve fit
C_2H_2-O_2 experimental data curve fit

Fig. 22

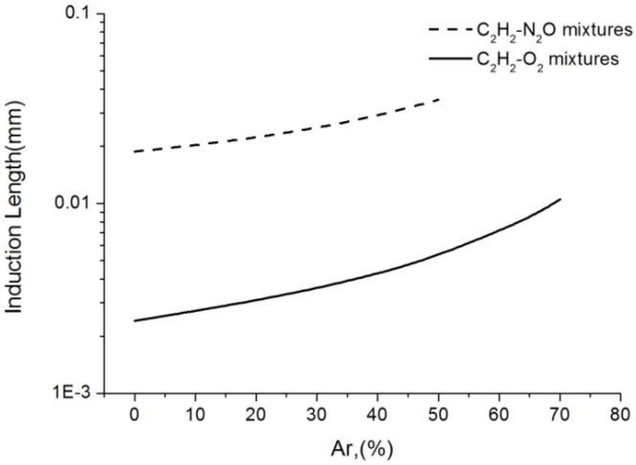

C_2H_2-N_2O mixtures
C_2H_2-O_2 mixtures
Induction Length(mm)
0.1
0.01
1E-3
0
10
20
30
40
50
60
70
80
Ar,(%)

Fig. 23